# Mean and Oscillating Plasma Flows and Turbulence Interactions across the L-H Confinement Transition

G.D. Conway, C. Angioni, F. Ryter, P. Sauter, J. Vicente[1], and the ASDEX Upgrade Team

*Max-Plank-Institut für Plasmaphysik,*

*EURATOM-Association IPP, D-85748, Garching, Germany*

[1]*Instituto de Plasmas e Fusão Nuclear,*

*Associação Euratom-IST, Lisboa, Portugal*

(Dated: July 23, 2010. Revision: January 12, 2011)

## Abstract

A complex interaction between turbulence driven $E \times B$ zonal flow oscillations, i.e. geodesic acoustic modes (GAMs), the turbulence, and mean equilibrium flows is observed during the low to high (L-H) plasma confinement mode transition in the ASDEX Upgrade tokamak. Below the L-H threshold at low densities a limit-cycle oscillation forms with competition between the turbulence level and the GAM flow shearing. At higher densities the cycle is diminished, while in the H-mode the cycle duration becomes too short to sustain the GAM, which is replaced by large amplitude broadband flow perturbations. Initially GAM amplitude increases as the H-mode transition is approached, but is then suppressed in the H-mode by enhanced mean flow shear.

PACS numbers: 52.35.Ra, 52.30.-q, 52.55.Fa, 52.70.Gw, 52.25.Gj

The role of turbulence driven zonal flows (ZFs) in the formation of energy and particle transport barriers is a key issue in many branches of fluid dynamics, particularly in magnetically confined plasmas (e.g. reviews [1–3]). Fundamental to the creation of transport barriers and the transition to improved plasma confinement states is the reduction of turbulence by flow shearing [4]. Here, both large-scale *mean* equilibrium (i.e. pressure gradient $\nabla P$ and external momentum driven) $E \times B$ flows and fine-scale *zonal* (e.g. turbulent Reynolds stress driven) flows play active, but different, roles [5].

Further, ZF models, such as the predator-prey model of Kim and Diamond [6], suggest a complex interaction between the ZFs, the turbulence, and mean $E \times B$ equilibrium flows. For example, in magnetic confinement fusion devices, before and during the edge transport barrier formation and the transition from low confinement (L-mode) to high confinement (H-mode), the mean flow shear is generally weak so that the GAM (geodesic acoustic mode - a few kHz coherent ZF oscillation which supplants the more core localized zero-mean-frequency ZF) may provide the dominant shearing effect - perhaps even triggering the shear-flow turbulence suppression feedback loop. As the H-mode forms the mean equilibrium flow shear grows with the steepening edge $\nabla P$ and eventually becomes dominant, suppressing both the turbulence and the GAM. This hypothesis is consistent with experimental observations, for example increased turbulence driven Reynolds stress in the HT-6M tokamak [7], enhanced low frequency edge turbulence coupling, prior to and during L-H transitions, in the DIII-D tokamak [8], and increased low frequency flow fluctuations in the TJ-II stellarator H-mode [9]. The impact of the mean flow on the ZF/GAM spectrum has also been noted in recent torque (toroidal rotation) scans performed on DIII-D [10]. It is also evident in the fact that the GAM, which is universally observed in ohmic and additionally heated L-mode regimes, remains suppressed in the H-mode [11], even when the edge turbulence level recovers later in H-mode due to the steepening edge gradients.

In this Letter we report new measurements from the ASDEX Upgrade tokamak which clearly demonstrate the role and importance of both the oscillating and mean flow shears and their interaction in triggering and maintaining confinement mode transitions in a fusion relevant device. Using microwave Doppler reflectometry to directly measure the $E \times B$ flow and its fluctuations with high spatial (few mm radially) and temporal (sub microsecond) resolution, the build-up of the edge GAM is observed; leading to the onset of sustained limit cycle oscillations (a feature predicted by predator-prey models) at low plasma collisionalities

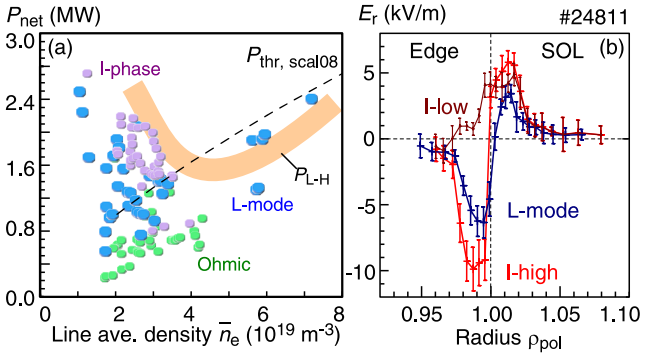


FIG. 1: (color online). (a) GAM existence plot in terms of $P_{\rm net}$ vs central line average density. (b) Edge radial electric field $E_{\rm r}$ profiles for L ($P_{\rm ECH} = 0.35$ MW) and I phase (1.1 MW) #24811, $B_{\rm T} = -2.3$ T, $I_{\rm p} = 0.8$ MA, $q_{95} \sim 4.5$, $\bar{n}_{\rm e} = 3 \times 10^{19}$ m$^{-3}$, $T_{\rm eo} \sim 2.4$ keV and favorable lower X-point.

$\nu^* \propto n_{\rm e}/T_{\rm e}^2$ (low plasma density $n_{\rm e}$ and/or high electron temperature $T_{\rm e}$); and finally the suppression of the GAM and turbulence as the mean equilibrium flow shear strengthens. In the limit-cycle phase the presence of a critical threshold for the onset of the turbulence driven flow, and the competing turbulence suppression by the flow shear are revealed for the first time.

Doppler reflectometry is a hybrid diagnostic combining the turbulence wavenumber selectivity of coherent scattering with the radial localization of microwave reflectometry [12, 13]. Tilting the reflectometer transceiver antennae obliquely to the plasma surface (in a plane *perpendicular* to the magnetic field) makes the diagnostic sensitive to density fluctuations satisfying the Bragg backscatter condition $k_\perp = -2k_{\rm o}N_\perp \approx 2k_{\rm o}\sin\theta_{\rm o}$, where $k_{\rm o}$ is the microwave probing wavenumber, $N_\perp$ the plasma refractive index at the reflection layer and $\theta_{\rm o}$ the antenna angle to the plasma surface. The measured fluctuation spectrum $S(f)$ is Doppler shifted $f_{\rm D} = u_\perp k_\perp/2\pi$ proportional to the fluctuation velocity $u_\perp = v_{E\times B} + v_{ph}$ (plasma $E_{\rm r} \times B$ plus turbulence phase velocity). Generally $v_{E\times B} \gg v_{ph}$, hence fluctuations in the radial electric field $E_{\rm r} \simeq -u_\perp B$ appear directly in the Doppler shift, while the Doppler peak intensity $S_{\rm D}$ is proportional to the turbulence level at the probed $k_\perp$ [11]. The measurements reported here were obtained with an X-mode $50-75$ GHz tunable frequency reflectometer with 20 MHz signal sampling, located below the tokamak outer mid-plane [14].

GAMs are most clearly observed at low plasma densities and high safety factors $q$ [15] due to weaker collisional and Landau damping [1]. Figure 1(a) shows a GAM existence

diagram in terms of net heating power $P_{\rm net}$ vs central line averaged plasma density $\bar{n}_{\rm e}$ for ohmic and L-mode heated plasmas. GAMs are not observed in the H-mode. Overlaid are the predicted (dash-line) and experimentally measured (curve) L-H power threshold showing two branches, see [16] for details. The GAM appears as a coherent peak in the $f_{\rm D}$ ($\tilde{E}_{\rm r}$) spectrum - cf. figure 5(a) in L-mode. Note the absence of coherent low frequency ZF activity, either as a peak or broadening of the spectra around zero frequency. The spectra continues to be flat down to the lowest spectral resolution investigated (a few tens of Hz).

From the low density L-mode (edge $\nu^*_{\rm edge} \sim 1$) raising either the heating power or the density causes the turbulence to rise across the whole edge region and to begin pulsating at around $2-4$ kHz (sometimes with a slower sub-pulse activity of a few hundred Hz) with an on-off duty cycle of less than 50%. This *intermediate* state (labeled I-phase) is not transitory but can be maintained for the entire discharge. Observations from many discharges confirm that the L to I-phase is a sharp transition with a well defined threshold, while the full H-mode appears to evolve more softly from the I-phase. The turbulence pulsing extends across the plasma edge into the open flux surface scrape-off-layer (SOL). Figure 2 shows an example close to the power/density threshold where the discharge dithers between the L and I-phases - illustrated by the divertor tile shunt current ($\propto$ SOL flow). The transition from continuous L-mode turbulence to pulsing is shown below in the Doppler reflectometer spectrogram $S(f,t)$ from just inside the $E_{\rm r}$ minimum location at a normalized poloidal flux radius $\rho_{\rm pol} \sim 0.988$. Below are the corresponding (smoothed) traces of the $u_\perp$ velocity and fluctuation level $S_{\rm D}$ at the probed $k_\perp \sim 9.8$ cm$^{-1}$.

The $u_\perp$ and $S_{\rm D}$ pulsing are synchronized and display all the features of a limit cycle behaviour with a fast switching between an enhanced and a reduced fluctuation state in less than 1 $\mu$s, i.e. on the turbulence time scale. The GAM is also still present, however, only during the enhanced turbulence state. This is more clearly seen in figure 3 which shows an expanded time trace of (a) the instantaneous $E_{\rm r}$ (100 ns resolution), plus (b) smoothed $E_{\rm r}$ and turbulence level $S_{\rm D}$ traces over four pulses. The figure shows a sequence of events: (1) The turbulence rises between the pulses; (2) reaches a critical threshold (marked by the dashed lines) and triggers an exceedingly large GAM oscillation (3) together with a turbulence driven mean flow - indicated by the offset in the oscillation. (The peak-to-peak GAM flow oscillation amplitude during the pulse can exceed 100% of the mean flow - stronger than in the preceding L-mode. While earlier observations also point towards a $\nabla T_{\rm e}$ (drive)

threshold for the GAM onset [15], it is possible that the GAM is also enhanced by the mean flow. Note also that the pulse frequency is generally less than a quarter of the GAM frequency so generally only a couple of GAM periods are visible.) Then (4), the resultant enhanced flow shearing affects the turbulence, which now begins to reduce. On reaching the critical threshold (there may be some hysteresis) the GAM switches off and the mean $E_{\rm r}$ well disappears, and in this case even reverses to become positive. This represents a substantial cyclic variation in the $E_{\rm r} \times B$ flow. Figure 1(b) shows the cyclic variation in the $E_{\rm r}$ profile (I-high and I-low) for a typical discharge with $P_{\rm ECH} = 1.1$ MW electron cyclotron heating power, together with an L-mode phase (0.35 MW). There is no equivalent modulation in the electron pressure gradient $\nabla P_{\rm e}$. Similar poloidal flow reversal observations were recently observed using gas-puff imaging on NSTX tokamak just prior to the L-H transition [17].

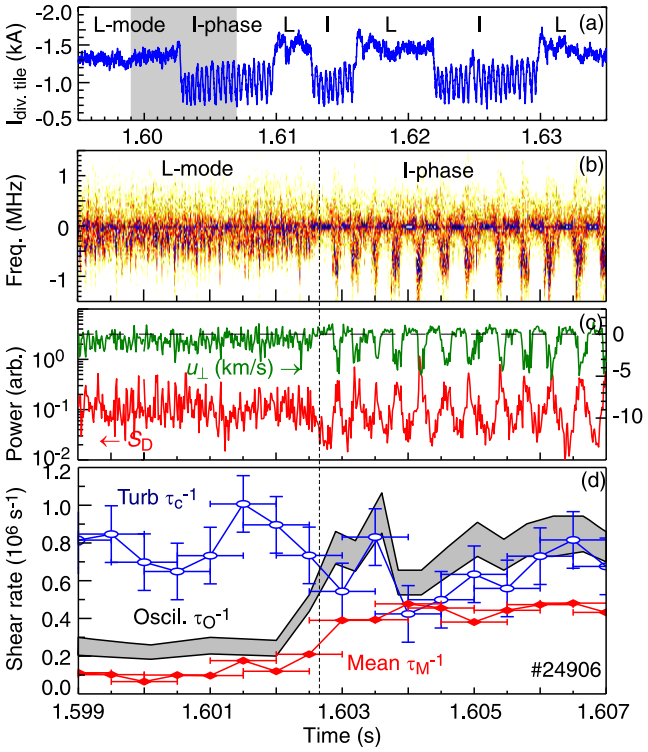


FIG. 2: (color online). (a) Time trace of divertor shunt current, (b) expanded reflectometer spectrogram $S(f,t)$ - darker colors for higher intensity, with (c) corresponding $u_\perp$ velocity and fluctuation level $S_{\rm D}$, and (d) estimated mean & oscillatory shearing rates and turbulence decorrelation rate $\tau_{\rm c}^{-1}$ across the L to I-phase. $B_{\rm T} = -2.3$ T, $I_{\rm p} = 1.0$ MA, $q_{95} \sim 4$, $\bar{n}_{\rm e} = 2.8 \times 10^{19}$ m$^{-3}$, $T_{\rm eo} \sim 3$ keV, $P_{\rm ECH} = 1.0$ MW.

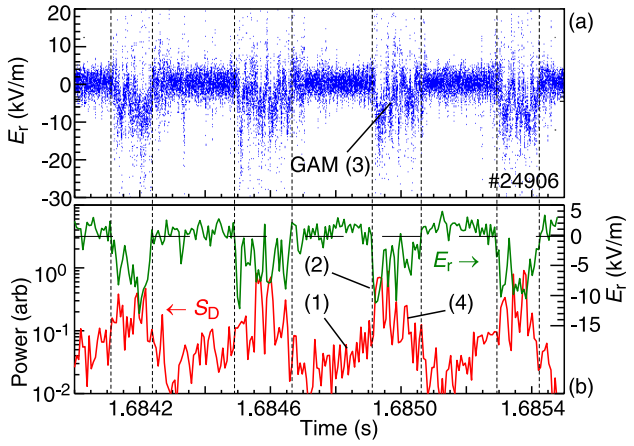


FIG. 3: (color online). (a) Instantaneous $E_r$ time trace over several pulses showing GAM oscillation, plus (b) smoothed $E_r$ and turbulence level $S_D$ showing (1) rising turbulence, (2) threshold, (3) GAM and (4) turb. suppression for #24906.

On the equilibrium time scale (i.e. ms) the enhanced turbulence driven flow (deeper edge negative $E_r$ well) supports a stronger edge pressure gradient, and hence higher energy confinement factors. In this discharge there is a steepening of the edge $T_e$ gradient but no evident H-mode pedestal formation. Note also the inward movement of the $E_r$ well (minimum) position and the consequent steepening of the positive and negative $E_r$ shear regions. This $E_r$ well movement is typical with improving energy confinement in L as well as H-mode conditions.

The role of the GAM shearing is demonstrated in figure 2(d) with estimates of the mean flow shearing rate $\tau_M^{-1} = \Delta u_\perp / L_r$ (red points) where $\Delta u_\perp$ the flow velocity step across the shear layer [4] and $L_r$ is the radial turbulent eddy size (correlation length approximated by the negative shear layer width); the corresponding flow oscillation shearing rate $\tau_O^{-1} = \sigma_{u\perp} / L_r$ (grey shaded curve) where $\sigma_{u\perp}$ is the flow standard deviation, together with the turbulence decorrelation rate $\tau_c^{-1}$ (open blue points) from the Doppler amplitude fluctuations. The horizontal bars indicate the averaging period. The $\sigma_{u\perp}$ tends to over estimate the effective GAM shearing in L-mode, but under estimates the GAM peak-to-peak amplitude during the I-phase pulses. Note that all three parameters are *local*, i.e. non-poloidally averaged, estimates at the same tokamak measurement location, and that the turbulence $\tau_c^{-1}$ is dominated by the probed $k_\perp$. Nevertheless, the figure shows that both the mean and oscillatory shear rates are well below the turbulence $\tau_c^{-1}$ in L-mode, but converge with the

onset of the pulsing. Of the two, it is $\tau_{\rm O}^{-1}$ which exceeds $\tau_{\rm c}^{-1}$ and then subsequently tracks it - thus maintaining the limit cycle behaviour.

The (equilibrium time scale) GAM amplitude initially increases with heating power. This is shown in figure 4(a & b) where a neutral beam injection (NBI) power ramp is applied in addition to the background ECH power. The GAM amplitude $A_{\rm GAM}$ (peak-to-peak velocity [15]) averaged over 100 ms, close to the GAM inner zonal boundary, begins to increase with the onset of the I-phase 50% duty-cycle pulsing; coincident with a bifurcation in the GAM frequency and the mean $E \times B$ flow ramping. However, the GAM eventually decreases as the mean flow shear strengthens. This effect is shown more clearly in figure 5. Here the ECH power is higher at 1.4 MW and the I-phase transition is triggered earlier at 1.65 s by the density ramp. The mean $E_{\rm r}$ well depth jumps from $-5.5$ to $-8.9$ kV m$^{-1}$ with a corresponding increase in the energy confinement factor $H_{98} = \tau_{\rm E}/\tau_{\rm Escale}$ from 0.6 (L) to 0.7 (I). In figure 5(b) the $f_{\rm D}$ spectrum (14 ms averaged) shows a weaker GAM peak, although the GAM during the pulse remains stronger than the 3kHz pulse perturbation. Around 2.37 s, the pulsing begins to diminish and clear, but weak ELM-free, H-mode $T_{\rm e}$ and $T_{\rm i}$ temperature pedestals form. The $D_\alpha$ emission drops slightly (reduced particle recycling) and the mean $E_{\rm r}$ well deepens, reaching $-24.5$ kV m$^{-1}$ with $H_{98} \approx 0.8$ indicating a transition to a mean flow shear dominated regime. This is confirmed by the local shear rate estimates shown in figure 5(f) where the rising mean flow $\tau_{\rm M}^{-1}$ crosses the turbulence decorrelation

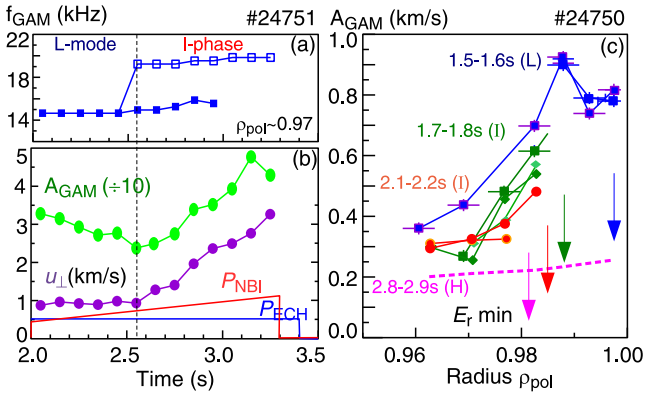


FIG. 4: (color online). Evolution of (a) GAM frequency (b) GAM amplitude $A_{\rm GAM}$ and $u_\perp$ flow velocity with heating power #24751; $B_{\rm T} = -2.4$ T, $I_{\rm p} = 1.0$ MA, $q_{95} \sim 4$, $\bar{n}_{\rm e} = 2.6 \times 10^{19}$ m$^{-3}$, $T_{\rm eo} \sim 3$ keV, $P_{\rm ECH} = 0.6$ MW plus $P_{\rm NBI}$ ramp. (c) Evolution of GAM amplitude profile during L-I-H mode transition, plus $E_{\rm r}$ well position (arrows) in #24750.

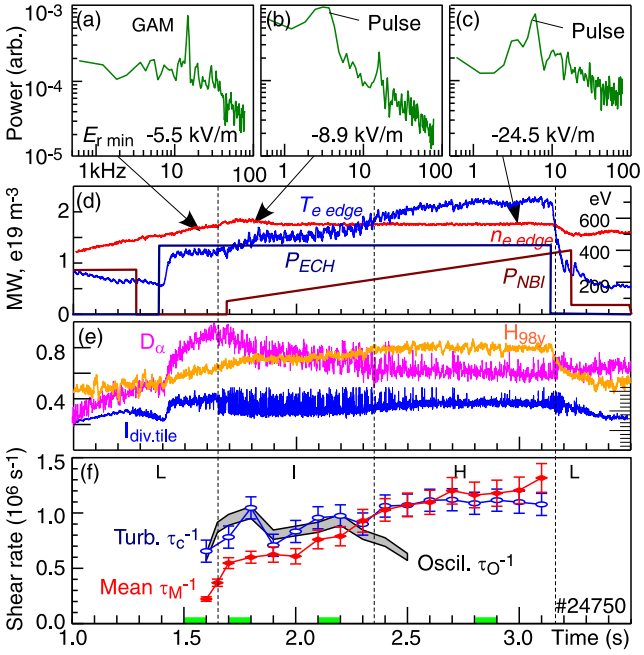


FIG. 5: (color online). Time averaged $f_{\rm D}$ spectra for (a) L, (b) I and (c) H-mode phases around $E_{\rm r}$ minimum at $\rho_{\rm pol} = 0.988$ , plus (d) & (e) parameter traces and (f) shearing rates of #24750; $B_{\rm T} = -2.3$ T, $I_{\rm p} = 1.0$ MA, $q_{95} \sim 4$, $\bar{n}_{\rm e} = 2.8 \times 10^{19}$ m$^{-3}$, $T_{\rm eo} \sim 5$ keV, $P_{\rm ECH} = 1.4$ MW plus $P_{\rm NBI}$ ramp, lower single-null with favorable $\nabla B$ X-point direction.

rate coincident with the crossing of the diminishing oscillatory $\tau_{\rm O}^{-1}$ shear rate. At this point a GAM is no longer observed anywhere in the edge region. There is also a qualitative change in the density turbulence behaviour, which drops across the edge and becomes more intermittent with short, semi-random pulses. In figure 5(c) the intermittency peak rises to $5.5 - 6$ kHz and the duty cycle drops to less than 30%. Essentially the turbulence pulses become too short to sustain a complete GAM period. Overall, the GAM disappears into a rising spectral background, i.e. the $E_{\rm r} \times B$ flow spectral power moves out of the coherent GAM into enhanced random broadband flow fluctuations [13].

With increasing mean flow shear the radial zonal extent of the GAM is also reduced. Figure 4(c) shows the $A_{\rm GAM}$ radial profile evolution for the same discharge as in figure 5. As the confinement improves the $E_{\rm r}$ well moves inward as it deepens (indicated by the arrows at the respective times), coinciding with the outer extent of the GAM eroding, before it disappears below the rising background level (dashed line). The GAM is only observed in the negative $E_{\rm r}$ shear region, which again shows the link between the mean and oscillating

flows.

Finally, with increasing plasma density both the GAM and limit-cycle/pulse frequencies decrease - the GAM due to decreasing $T_e$ and the cycle most likely due to collisional ZF damping [2]. To date, the limit cycle pulsing has not be observed for the high density L-H threshold branch, i.e. $\bar{n}_e > 5 \times 10^{19}$ m$^{-3}$. Although the GAM can be just as intense here, its reduced frequency relative to the pulse might effectively close-out the I-phase regime leading to a more rapid transition to the H-mode.

To summarize, evidence is presented of the GAM/ZF - mean flow - turbulence interaction where the GAM flow shearing dominates in the turbulent, low mean flow shear L-mode, but is suppressed in the quiescent, high mean flow shear H-mode. In between, at low plasma density a limit-cycle oscillation forms with competing turbulence drive and enhanced flow shearing. With increasing input power the GAM amplitude first rises, but is then suppressed and radially eroded by the increasing mean flow shear. The picture is of close interaction and inter-dependence of the equilibrium and turbulence driven flows - which acting together appear to trigger the velocity shear feedback loop believed to be responsible for the H-mode formation. In the H-mode the coherent GAM is replaced by broadband flow fluctuations, which may also play a role in decorrelating the turbulence [18].

We thank E.Poli for assistance with the beam-tracing software; G.Tynan, P.Diamond, R.McDermott, B.Scott and K.Hallatschek for fruitful discussions.

[1] P.H. Diamond, S-I. Itoh, K. Itoh and T. Hahm, Plasma Phys. Control. Fusion **47**, R35 (2005).

[2] K. Itoh *et al.*, Phys. Plasmas **13**, 055502 (2006).

[3] A. Fujisawa, Nucl. Fusion **49**, 013001 (2009).

[4] P.W. Terry, Rev. Mod. Phys. **72**, 109 (2000).

[5] G.R. Tynan, A. Fujisawa and G. McKee, Plasma Phys. Control. Fusion **51**, 113001 (2009).

[6] E.J. Kim and P.H. Diamond, Phys. Rev. Lett. **90** 185006 (2003).

[7] Y.H. Xu *et al.*, Phys. Rev. Lett. **84** 3867 (2000).

[8] R.A. Moyer *et al.*, Phys. Rev. Lett. **87** 135001 (2001).

[9] T. Estrada *et al.*, Plasma Phys. Control. Fusion **51**, 124015 (2009).

[10] G.R. McKee *et al.*, Nucl. Fusion **49**, 115016 (2009).

[11] G.D. Conway *et al.*, Plasma Phys. Control. Fusion **47**, 1165 (2005).

[12] M. Hirsch *et al.*, Plasma Phys. Control. Fusion **43**, 1641 (2001).

[13] G.D. Conway *et al.*, Plasma Fusion Res. **5**, S2005 (2010).

[14] G.D. Conway *et al.*, Plasma Phys. Control. Fusion **46**, 951 (2004).

[15] G.D. Conway and AUG Team, Plasma Phys. Control. Fusion **50**, 085005 (2008).

[16] F. Ryter *et al.*, Nucl. Fusion **49**, 062003 (2009).

[17] S.J. Zweben *et al.*, Phys. Plasma **17**, 102502 (2010).

[18] E.J. Kim and P.H. Diamond, Phys. Plasmas **11**, L77 (2004).